Supporting Information

Constructing efficient ion nanochannels in alkaline anion exchange membranes by *in-situ* assembly of poly (ionic liquid) in metal-organic frameworks

Zhen Li,[a,b] Wenyu Wang,[a] Yijing Chen, [a] Chuanye Xiong,[a] Guangwei He,[a,b] Ying Cao,[a b] Hong Wu,[a,b] Michael D. Guiver[a,c] and Zhongyi Jiang[a,b] *

*Key Laboratory for Green Chemical Technology, Ministry of Education of China, School of Chemical Engineering and Technology, Tianjin University, Tianjin 300072, China. * E-mail: zhyjiang@tju.edu.cn. Fax: +86 22 2350 0086. Tel: +86 22 2350 0086.*

Collaborative Innovation Center of Chemical Science and Engineering (Tianjin), Tianjin 300072, China

State Key Laboratory of Engines, School of Mechanical Engineering, Tianjin University, Tianjin 300072, China

I. Methods

II. Supplementary figures and table

Supplementary references

I. Methods

Measurement of mechanical properties. Mechanical properties of membranes were tested using a universal tension and compression test system (Yangzhou Zhongke Jiliang Ltd, China) with a stretching rate of 20 mm min^{-1}. Both fully hydrated and dry membranes were tested at room temperature.

Measurement of EDX spectrum. EDX spectra were carried out using the energy dispersive X-ray detector on the FESEM and the HRTEM, respectively.

Thermogravimetric measurement. Thermogravimetric measurements were carried out on NETZSCH-TG209 F3 instrument at the temperature range of 40-800 ^{o}C in air with a heating rate of 10 ^{o}C min^{-1}. Membrane samples cut in to small pieces were used for the test.

Measurement of water uptake and area swelling. Membrane samples were dried at 60 ^{o}C under vacuum until constant weight (W_{dry}, g). Their areas (A_{dry}, cm^2) were measured after drying. After immersing membranes in water at different temperatures until fully hydrated, their weights (W_{wet}, g) and areas (A_{wet}, cm^2) of membranes were measured. Water uptake and area swelling were calculated using **Equation S1** and **S2**, respectively.

$$\text{Water uptake (\%)} = \frac{W_{wet} - W_{dry}}{W_{dry}} \times 100\% \quad \text{(S1)}$$

$$\text{Area swelling (\%)} = \frac{A_{wet} - A_{dry}}{A_{dry}} \times 100\% \quad \text{(S2)}$$

Calculation of ion concentration and effective mobility. According to Holdcroft's research on solid electrolytes,[S1, S2] the ionic conductivity of ion exchange membranes (IEMs) is the product of the Faraday's constant (F), ion concentration and effective mobility (μ, cm^2 s^{-1} V^{-1}), as shown in **Equation S8**. Ion concentration (a, mmol cm^3) is the molar mass of conductive groups per unit volume, which was calculated using **Equation S3**. Effective mobility is the combination of intrinsic mobility of ion and properties of channel morphology (e.g. tortuosity of ion channel, number of channels, spatial proximity of ion groups etc.), which provides an insight into the ion transport efficiency in channels and can be calculated

using **Equation S5.**

$$a = \frac{\mathrm{IEC} \times m}{V} = \frac{\mathrm{IEC} \times \rho \times V_{\mathrm{dry}}}{V} = \mathrm{IEC} \times \rho \times \mathrm{VS} \quad \text{(S3)}$$

$$\sigma = Fa\mu \quad \text{(S4)}$$

$$\mu = \frac{\sigma}{Fa} \quad \text{(S5)}$$

Where

m (g) is mass of dry membrane;

ρ (g cm^3) is mass density of dry membrane;

V_{dry} (cm^3) is the volume of dry membrane;

V (cm^3) is the volume of membrane under the testing condition;

VS is volume swelling of membrane.

Measurement of alkaline stability of membranes. Alkaline stability of membranes in hot alkaline solution was assessed. Membranes were immersed in 1 M sodium hydroxide solution at 60 ^{o}C for 24 h and then washed with abundant water. The hydroxide conductivity of membranes was tested before and after to evaluate the alkaline stability of membranes.

Measurement of methanol permeability. Methanol permeability (P, cm^2 s^{-1}, tested in 2 M aqueous methanol) was measured using a glass diffusion cell separated into two compartments, between which the membrane was sandwiched. One compartment was filled with 2 M methanol, and the other compartment was filled with water. The methanol concentration in the water compartment was measured at set intervals using a gas chromatography (Agilent 6820). Methanol permeability (P, cm^2 s^{-1}) was calculated from **Equation S6**.

$$P = \frac{SV_B l}{AC_{A0}} \quad \text{(S6)}$$

Where

S is the slope of the straight line of methanol concentration in the water compartment versus time;

V_B is the volume of the solution in the water compartment;

l is the membrane thickness;

A is effective membrane area which is calculated by the inner diameter of the diffusion cell;

C_{Ao} is feed methanol concentration.

II. Supplementary figures and tables

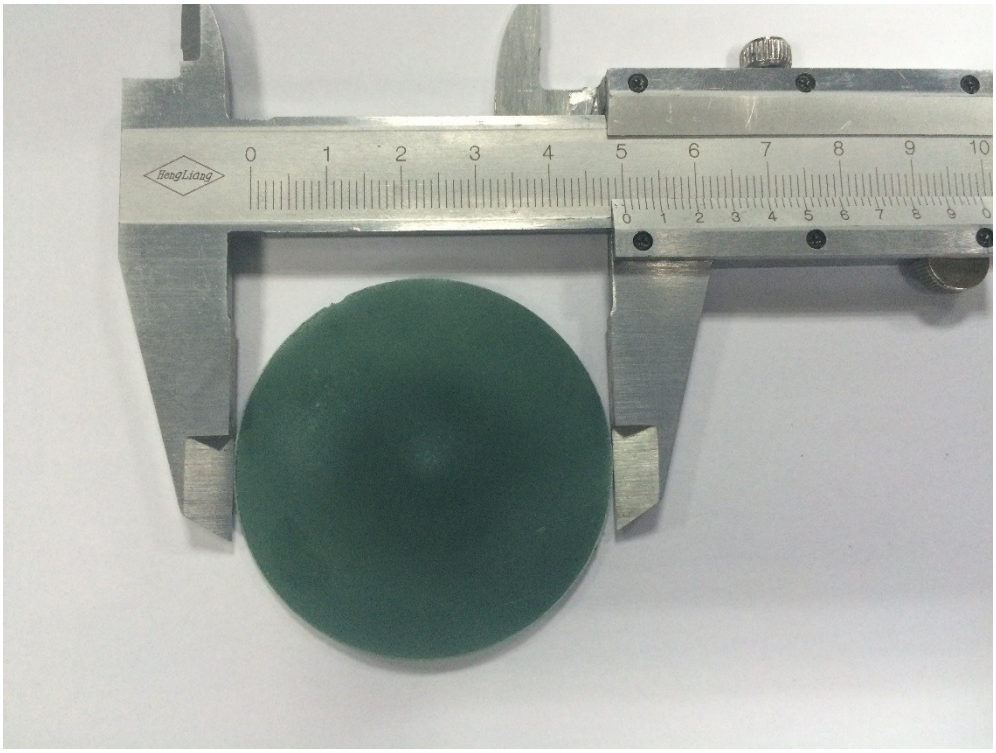

Figure S1. Photograph of PIL@MIL-mem.

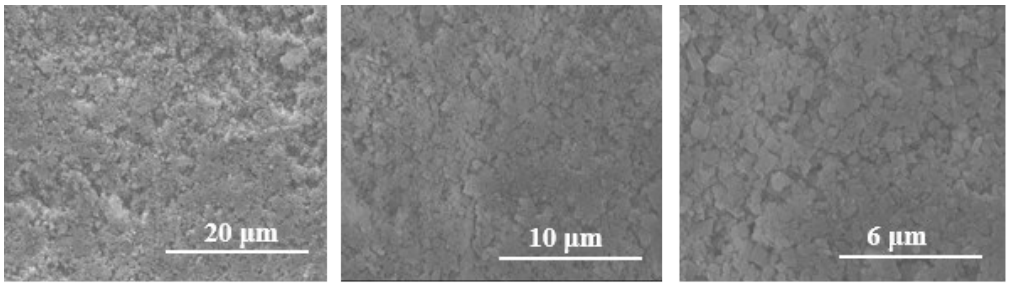

Figure S2. FESEM images of cross section of PIL@MIL-mem at different magnifications.

PIL@MIL nanoparticles are closely packed with each other, and preserved their initial morphologies in PIL@MIL-mem, which is dense and defect-free.

1 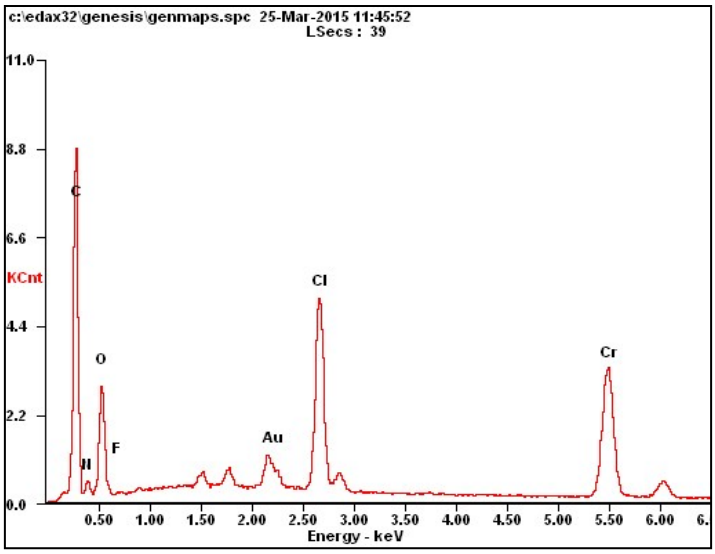

2 **Figure S3. EDX spectrum of PIL@MIL.**

3 PIL@MIL consists of C, O, N, Cl and Cr. The existence of N and Cl indicates the

4 successful entrapment of PIL.

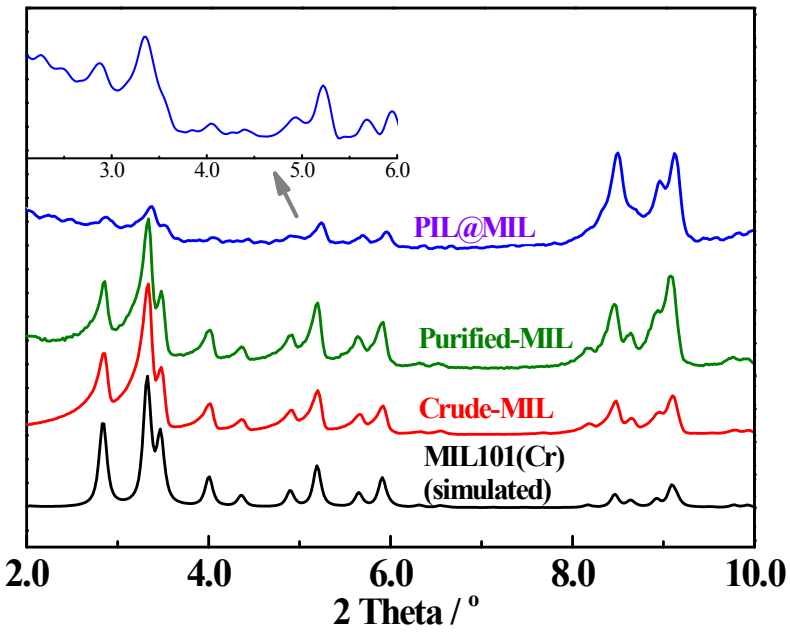

1

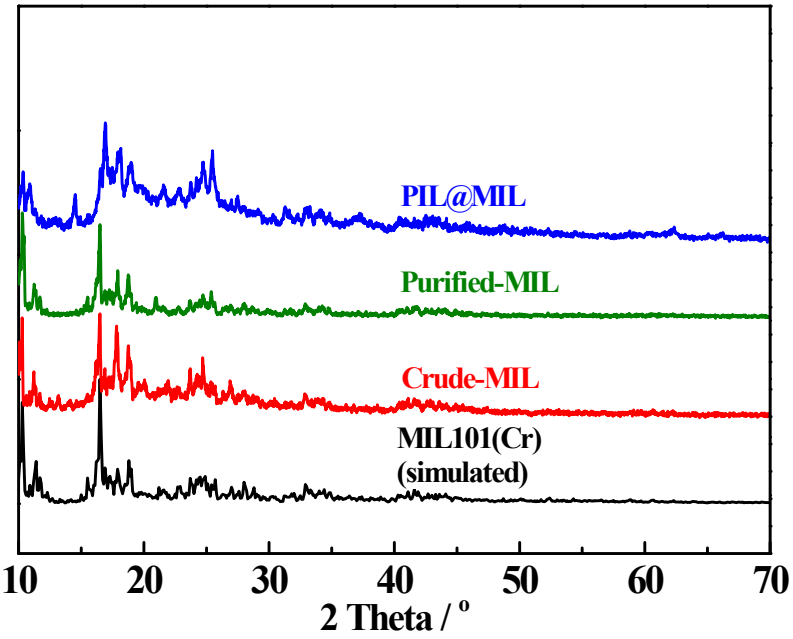

2

3

4 **Figure S4. XRD patterns of Crude-MIL, Purified-MIL, PIL@MIL and the simulated**

5 **patterns at the angular range of 2-10° and 10-70°.**

6

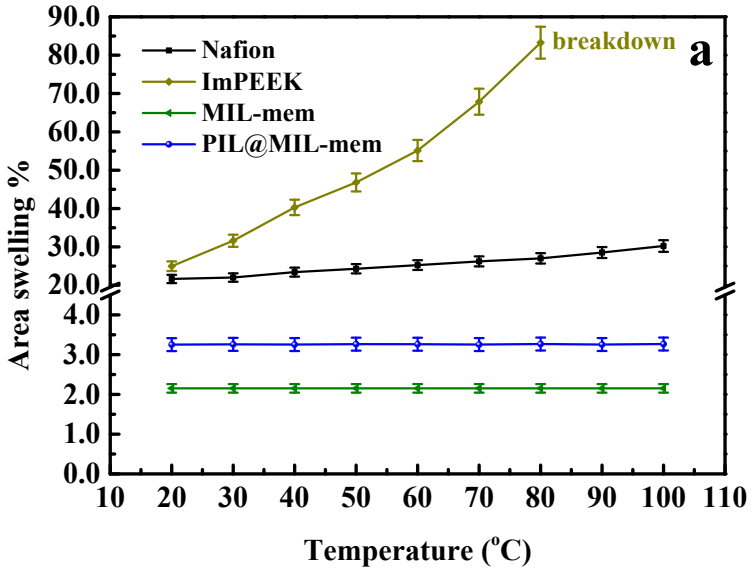

1

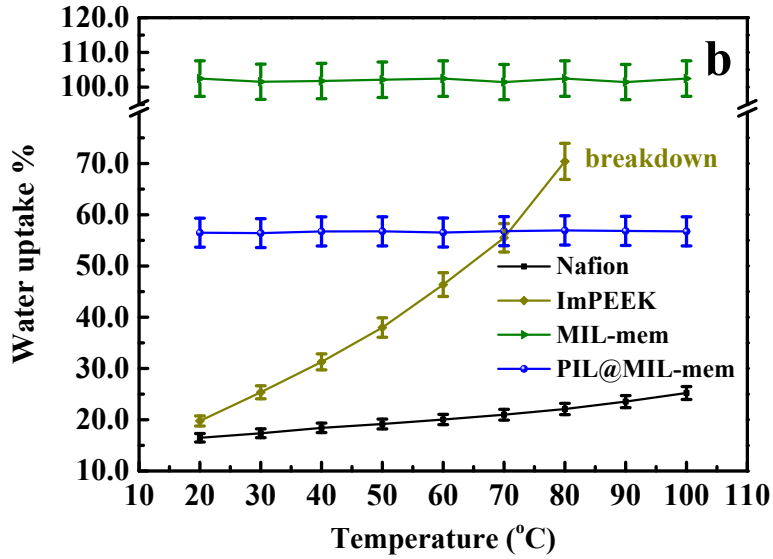

2

3

4 **Figure S5. Area swelling (a) and water uptake (b) of membranes.**

5 Area swelling of MIL-mem and PIL@MIL-mem is very low, which is respectively only
6 2.15% and 3.25%. The rigid framework of MIL101 does not swell, and any observed swelling
7 of PIL@MIL-mem is only the result of interpenetration of water molecules into the
8 binder/MIL101 nanoparticle interfaces. Due to the excellent mechanical property of SEBS
9 (binder), the area swelling of MIL-mem and PIL@MIL-mem is restrained effectively. By
10 contrast, area swelling of Nafion and ImPEEK are 21.64% and 24.94%, respectively, at 20 °C.
11 As temperature increases, area swelling of Nafion increases to 30.29% at 100 °C, and that of

ImPEEK sharply increases to 83.26 % at 80 °C. The low area swelling of PIL@MIL-mem implies improved compatibility of membrane/catalyst interface as well as elevated stability of membrane electrode assembly.

Due to the huge pore volume of MIL101, PIL@MIL-mem and MIL-mem show high water uptake although their area swelling are very low. PIL occupies some space in the pores of MIL101, thus PIL@MIL-mem shows lower water uptake than MIL-mem. In contrast, polymer membranes absorb water by swelling, thus water uptake of both ImPEEK and Nafion show an identical trend with area swelling.

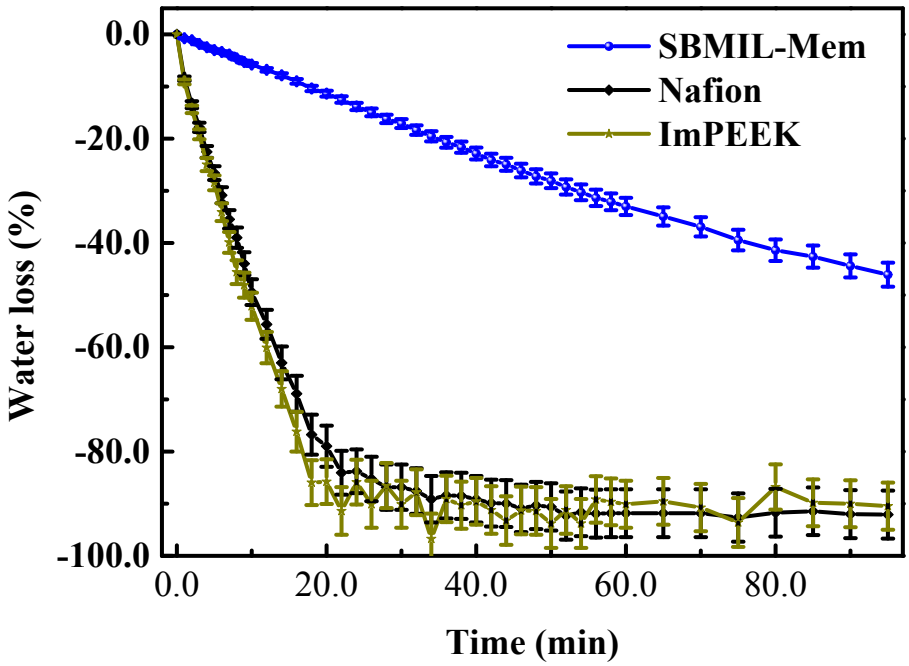

Figure S6. Water loss curve of PIL@MIL-mem at 20 % relative humidity, 30 °C.

Much effort has been devoted to enhance the water retention properties of PEMs/AEMs because water plays an important role in the proton/hydroxide ion transport, which affects the dissociation of proton/hydroxide ion, the formation of hydrogen-bonding network and the diffusion of ions. PIL@MIL-mem shows higher water retention than polymer membranes, which only lose 45% of water after 95 min. By contrast, both Nafion and ImPEEK lose about 90% of water after 25 min. According to the Kelvin equation, $\ln RH=\gamma V_m/(rRT)$, the saturated vapor pressure of water will increase in nanopores, which prevents the escape of water from the pores of MIL101. In addition, the strong hydrophilicity of PIL also may be conducive to the water retention. A higher water retention endows PIL@MIL-mem with potential application at low humidity.

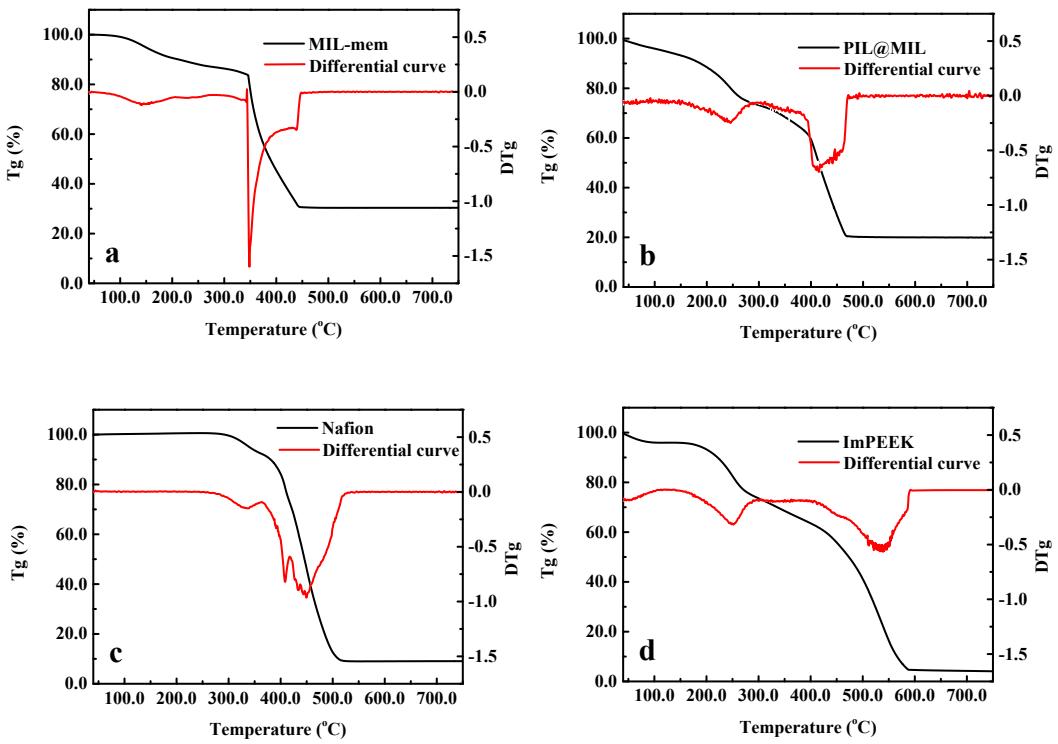

Figure S7. Thermogravimetric curve of (a) Purified-MIL; (b) PIL@MIL; (c) Nafion; (d) ImPEEK.

The PIL@MIL decomposes in three steps. The first step below 200.0 °C results from the volatilization of water and other solvents trapped in the matrix. The second step from 200.0 to 282.0 °C is ascribed to the decomposition of imidazolium groups, which is in accordance with the decomposition process of ImPEEK (Figure S7d). The third step from 373 to 468.0 °C is ascribed to the decomposition of organic ligands of MIL101, which is accordance with the decomposition process of Purified-MIL. It can be concluded that PIL@MIL preserves the thermal stability of hydroxide conductive groups, and can tolerate the normal operating condition (<150.0 °C) for practical application of low and medium temperature fuel cells.

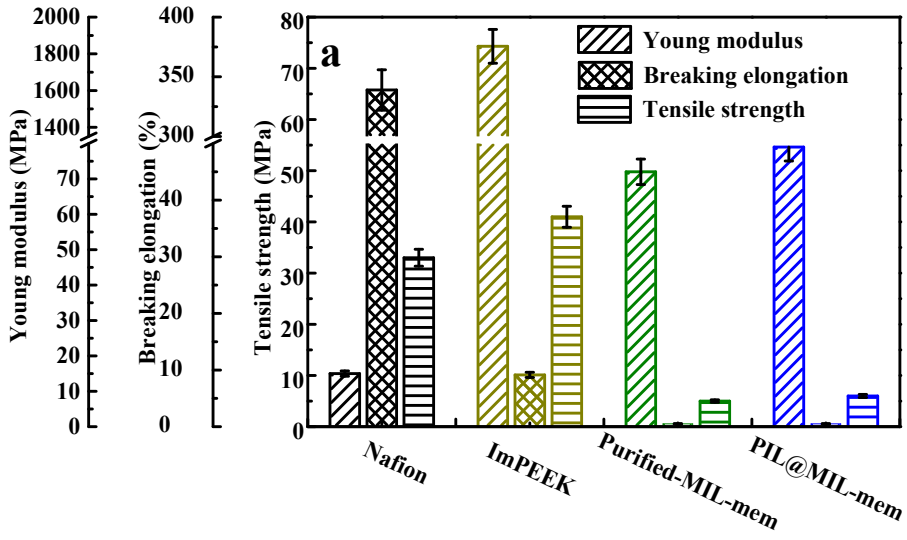

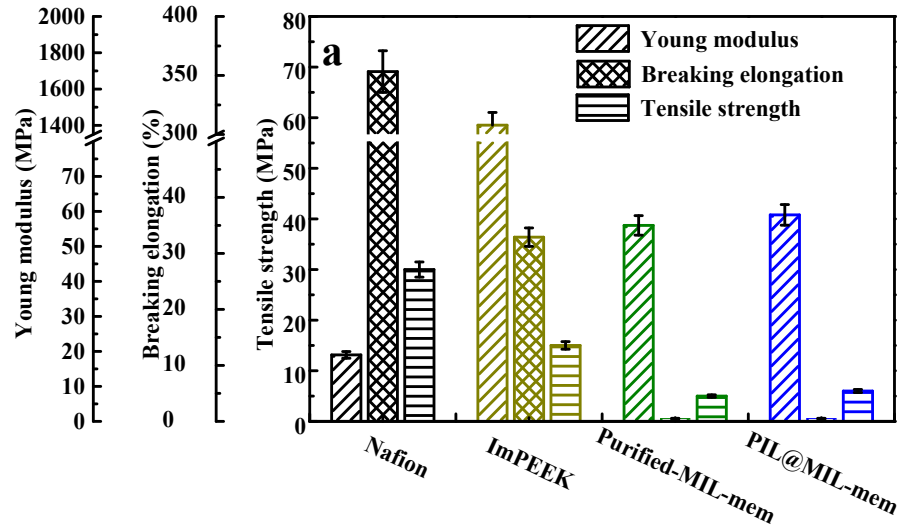

Figure S8. Mechanical properties of Nafion, ImPEEK, MIL-mem and PIL@MIL-mem under (a) dry conditions; (b) wet conditions.

Under dry conditions, the tensile strengths of MIL-mem and PIL@MIL-mem are 5 and 6 MPa, respectively. By contrast, the tensile strength of Nafion and ImPEEK are 33 MPa and 44 MPa, respectively. In addition, polymer membranes exhibit good flexibility.

Under wet condition, the mechanical properties of MIL-mem and PIL@MIL-mem shows little change, which is quite close to that under dry condition. By contrast, although the flexibility of polymer membranes is enhanced, the tensile strength of polymer membranes is weakened by water molecules. The tensile strength of Nafion decreases to 30 MPa, and that of ImPEEK sharply decreases to 15 MPa.

In conclusion, the overall mechanical properties of PIL@MIL-mem are worse than those of polymer membranes, which is an inherent shortcoming for inorganic membranes, and should be addressed in the future studies.

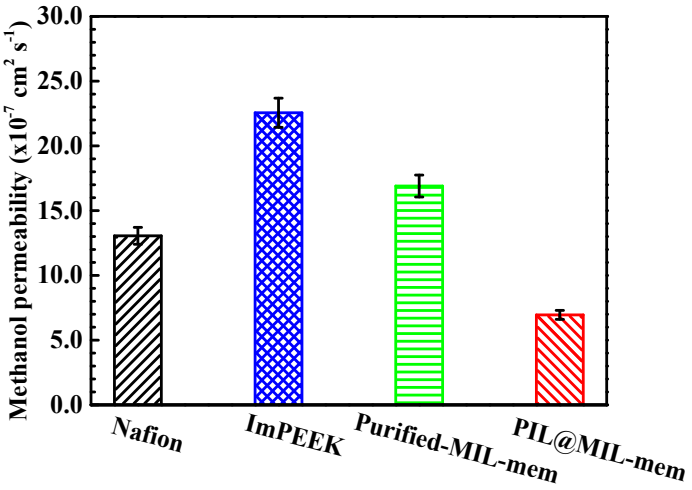

Figure S9. Methanol permeabilities of membranes.

In order to explore the application potential of MIL@PIL-mem in direct methanol fuel cell (DMFC), the methanol permeability of MIL@PIL-mem was measured at 30 °C, compared with those of ImPEEK and Nafion. Membranes for DMFC must simultaneously have high ionic conductivity and low methanol permeability. However, the ionic conductivity always has a strong trade-off relationship with methanol permeability, making it a challenge to fabricate membranes having both favorable conductivity and methanol-barrier properties.[36]Although the MIL-101 is highly porous, the PIL@MIL-mem shows a lower methanol permeability than many polymer membranes, which is attributed to two factors: 1) the pores of MIL-101 are blocked by the PILs, which are ionic electrolytes that favor ion transport of OH^- instead of methanol; 2) the framework of MIL-101 is rigid and swelling-free. According to Kreuer,[44] methanol can behave as a surfactant to weaken the interaction of the polymer backbone, enhancing the free volume of polymer membranes and aggravating the methanol permeability.

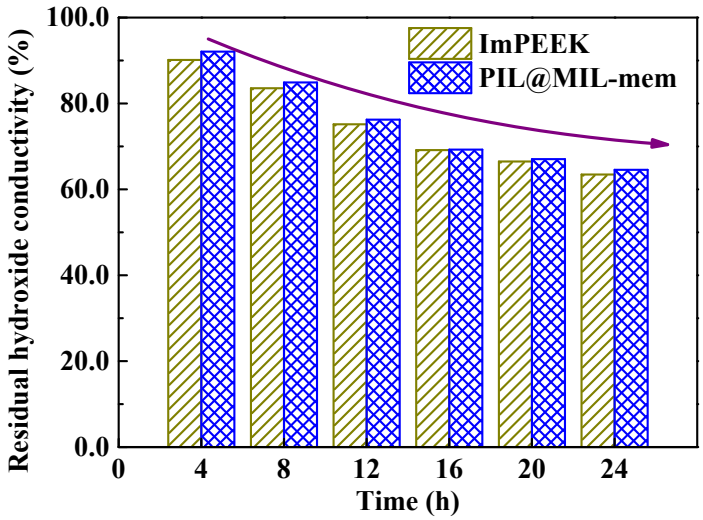

Figure S10. The alkaline stability of membranes.

This study aims at presenting a novel, generic approach to nanochannel construction using MOFs in AEMs; it does not address alkaline stability issue. Not surprisingly, PIL@MIL-mem shows a similar degradation trend as ImPEEK, which is ascribed to the Hofmann degradation reaction of imidazolium under alkaline condition. Utilization of alkaline conductive groups with higher stability will likely be a feasible solution to this problem. Further exploitations on MOF membranes with higher alkaline stability are ongoing.

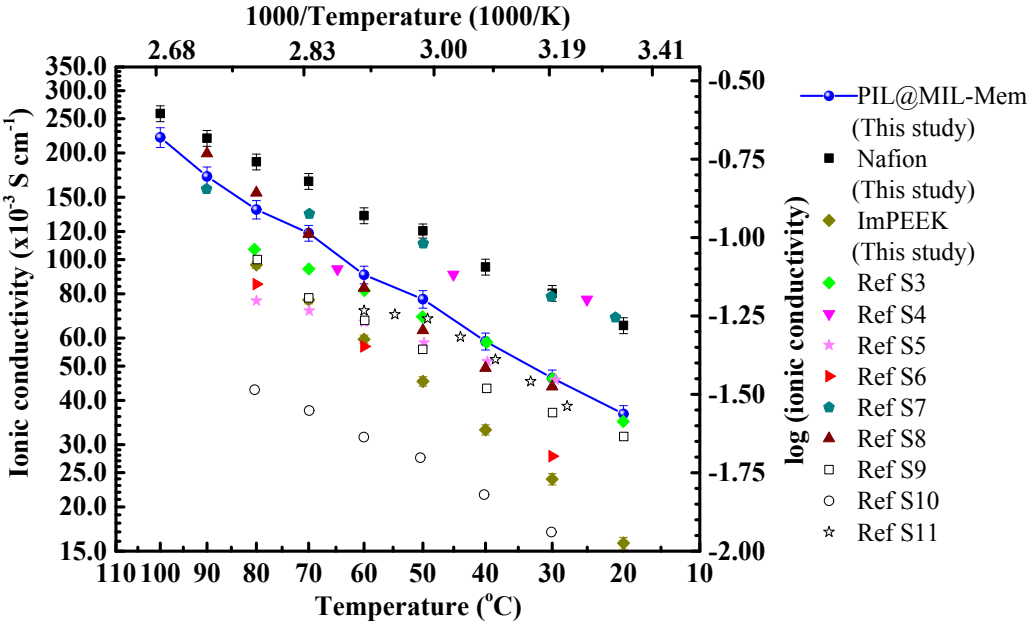

1

2 **Figure S11. Comparative hydroxide ion conductivities of membranes reported in this**

3 **study and in the literature**

Table S1 The illustration of conductivity, intrinsic mobility and mole conductivity of aqueous sodium hydroxide at 18 ^{o}C and different activities[S12]

Activity /mmol cm^{-3}	0.2522	0.5099	1.0420	1.3163	1.5961	2.1722	2.770
Conductivity / S cm^{-1}	0.0465	0.0887	0.1626	0.1954	0.2242	0.2729	0.3093
Intrinsic mobility / $x10^{-4}$ cm^2 $s^{-1}V^{-1}$	19.20	18.84	18.52	18.43	18.34	18.25	18.31
Mole conductivity / S cm^2 mol^{-1}	184.5	173.7	156.3	148.4	140.5	125.6	111.7

Table S1 lists the intrinsic mobilities and mole conductivities of aqueous sodium hydroxide at 18 ^{o}C and different activities. Although the mole conductivities of aqueous sodium hydroxide continue to decrease with the increased activities, the intrinsic mobilities remain similar.

References:

S1. T. J. Peckham and S. Holdcroft, *Adv. Mater.*, 2010, **22**, 4667-4690.

S2. T. J. Peckham, J. Schmeisser, M. Rodgers and S. Holdcroft, *J. Mater. Chem.*, 2007, **17**, 3255.

S3 J. Pan, C. Chen, Y. Li, L. Wang, L. Tan, G Li, X. Tang, L. Xiao, J. Lua and L. Zhuang, *Energy Environ. Sci.*, 2014, **7**, 354–360.

S4 H. Zarrin, J. Fu, G. Jiang, S. Yoo, J. Lenos, M. Fowler and Z. Chen, *ACS Nano*, 2015, **9**, 2028–2037.

S5 M. Tanaka, K. Fukasawa, E. Nishino, S. Yamaguchi, K. Yamada, H. Tanaka, B. Bae, K. Miyatake and Masahiro Watanabe, *J. Am. Chem. Soc.*, 2011, **133**, 10646–10654.

S6 J. Pan, Y. Li, J. Han, G. Li, L. Tan, C. Chen, J. Lua and L. Zhuang, *Energy Environ. Sci.*, 2013, **6**, 2912–2915.

S7 N. J. Robertson, H. A. Kostalik IV, T. J. Clark, P. F. Mutolo, H. D. Abruña and G. W. Coates , *J. Am. Chem. Soc.*, 2010, **132**, 3400–3404.

S8 J. Ran, L. Wu, B. Wei, Y. Chen and T. Xu, *Sci Rep-UK*, 2014, **4**, 6486–6490.

S9 C. Qu, H. Zhang, F. Zhang and B. Liu, *J. Mater. Chem.*, 2012,**22**, 8203-8207.

S10 Z. Si, Z. Sun, F. Gu, L. Qiu and F. Yan, *J. Mater. Chem. A*, 2014, **2**, 4413–4421.

S11 X. Lin, J. R. Varcoe, S. D. Poynton, X. Liang, A. L. Ong, J. Ran, Y. Li and T. Xu, *J. Mater. Chem. A,* 2013, **1**, 7262–7269.

S12 W. R. Bousfield, T. M. Lowry, *Phil. Trans. R. Soc. Lond. A*, 1905, 204, 253-322.